Assessment of Ball Milling as a Compounding Technique to Develop Nanocomposites of Poly(3-Hydroxybutyrate-co-3-Hydroxyvalerate) and Bacterial Cellulose Nanowhiskers

Jesús Ambrosio-Martin[a], María José Fabra[a], Amparo López-Rubio[a], Giuliana Gorrasi[b]*, Andrea Sorrentino[c] and Jose M. Lagaron[a]*

[a]Novel Materials and Nanotechnology Group, IATA-CSIC, Avda. Agustin Escardino 7, 46980 Paterna (Valencia), Spain.

[b]Department of Industrial Engineering, University of Salerno, via Giovanni Paolo II, 132 Fisciano (Salerno), Italy.

[c]Institute for Polymers, Composites and Biomaterials (IPCB), National Research Council (CNR), P.le Enrico Fermi 1, 80055 Portici, Italy.

*Author to whom the correspondence can be addressed

E-mail address: lagaron@iata.csic.es

+34 963900022 - fax: +34 963 636301

Running head

Assessment of Ball Milling to Develop PHBV / BCNW Nanocomposites

Abstract

The aim of this study was the assessment of high energy ball milling technique to develop poly(3-hydroxybutyrate-co-3-hydroxyvalerate) (PHBV) nanocomposites containing bacterial cellulose nanowhiskers (BCNW). Crystallization behaviour of PHBV/BCNW nanocomposites was studied under non-isothermal and isothermal conditions using differential scanning calorimetry (DSC). The changes in PHBV crystalline structure were also studied using X-ray diffraction. The results confirmed that BCNW acted as nucleating agents and, hence, favored the crystallization of the PHBV. The oxygen permeability of the nanocomposites was reduced by ~22% when compared to that of the neat PHBV. This work provides a new insight into the development of polyhydroxyalkanoate (PHA) composites by means of the high energy ball milling technique.

Keywords: Polyhydroxyalkanoates, Bacterial cellulose nanowhiskers, Bacterial cellulose nanocrystals, Oxygen barrier, Ball milling.

1. INTRODUCTION

Currently, there is a great interest in developing effective biodegradable materials to counteract the existing plastic waste management issues. Nowadays, in the food packaging area, the bio-based materials with greatest commercial potential are some biodegradable polyesters, which can be transformed using conventional plastic processing equipment. Among the most widely researched thermoplastic biodegradable materials, poly(lactic acid) (PLA) and polyhydroxyalkanoates (PHAs) present an interesting balance of properties, they are synthesized from renewable resources and have become commercially available. Specifically, PHAs are biopolyesters synthesized by a wide variety of microorganisms and degraded by numerous microorganism (bacteria, fungi and algae) in various ecosystems [1]. Due to their biodegradability, biocompatibility and adaptable mechanical properties, PHAs have been quickly identified as good candidates to replace fossil-based commodity polymers. However, widespread applications of PHAs are still hindered by several material drawbacks such as high material costs, relatively low barrier performance, poor thermal stability, brittleness and low crystallization rates.

The use of nanoparticles is attractive because they can act as nucleating agents, not only improving the polymer crystallization rates, but also increasing the mechanical, thermal and/or barrier performance of the composites. For instance, inorganic nano-fillers such as carbon nanotubes [2] and nanoclays [3,4] have demonstrated to increase the crystallization rate of poly(3-hydroxybutyrate-co-3-hydroxyvalerate) (PHBV), and enhance the stiffness and thermal stability of the nanocomposites. Moreover, improvements on the barrier properties of PHBV upon addition of nanoclays have also been reported with reductions of 76% and 32% in water and oxygen permeability respectively using 5 wt.% of filler [5]. However, the non biodegradable character of

these inorganic fillers make them non suitable in order to develop fully renewable materials.

Cellulose nanowhiskers (CNW) also called cellulose nanocrystals (CNC), which can be extracted from different sources, even from food by-products as recently reported [6], have attracted considerable attention as reinforcing agents in nanocomposites due to their attractive properties, such as low density, renewable character and biodegradability [7-9]. Several works have reported on the production of PHBV nanocomposites incorporating CNW attempting to improve the polymer matrix properties [6,9-12]. Nevertheless, CNW obtained from bacerial cultures, the so-called bacterial cellulose nanowhiskers (BCNW) have gained even more attention due to their high purity and outstanding properties [13,14]. Traditionally, solution casting has been the most extended method to prepare CNW-based nanocomposites. As it has been previously reported, this method is time-consuming, requiring repeated successive centrifugation steps [15], and it does not guarantee a good dispersion of the CNW because of the inherent difficulty to properly disperse these hydrophilic nanofillers in organic solvents [6], which have to be used in large amounts. In fact, one of the main drawbacks associated with the use of unmodified cellulose nanowhiskers as reinforcing agents is their very strong water sensitivity, which makes them difficult to disperse in non-polar media. As a consequence, the development of CNW-containing nanocomposites with improved properties remains as a great challenge and many scientific efforts are being put into it. Thus, several works have been published reporting different strategies to solve this problem, such as choosing the optimum solvent or chemically modifying the CNW surface in order to produce PHBV/CNW nanocomposites with improved properties [10,15,16]. The previous strategies have shown to result in better mechanical properties (up to 282% and 166% increase in the Young's Modulus and tensile strength

respectively) [11] and improved thermal stability up to 30 ºC [15,16] for PHBV nanocomposites reinforced with CNW. Moreover, a reduced water uptake and water vapour permeability was also obtained reaching improvements of 74% and 56%, respectively [16]. Despite such improvements, the casting technique used to develop these nanocomposites requires important amounts of organic solvents which are toxic and expensive and, moreover, it is not an appropiate and practical technique from the industrial applications point of view. Melt compounding techniques, such as extrusion or injection molding, are the most widely used processing techniques at industrial scale. However, regardless the polymer matrix, there is scarce literature about the production of CNW-containing nanocomposites throuth melt compounding methods. Again the challenge is to attain a good dispersion of CNW within the biopolymer matrix due to the hydrophobic nature of the most polymeric matrices resulting in poor interfacial interactions between filler and polymer. As previously reported, several alternatives have been successfully proposed to resolve the above disturbing problems, mainly based in the development of a initial compounded material which is used as masterbatch and subsequently diluted in melt state with different polymer matrices. For instance, the dispersion of CNW into PLA matrix has been improved using this strategy by several authors [13,17-20], with improvements in Young's modulus, tensile strength and oxygen and water vapour permeability up to 52%, 31%, 22% and 18%, respectively [19]. Furthermore, it has been recently published that PLA-cellulose nanofibrils nanocomposites were succesfully prepared by melt extrusion. A plasticizer was used as processing aid to facilitate the nanofiber dispersion and also the cellulose was feeded from a liquid medium [21], thus avoiding nanofiller agglomeration, which is in accordance with previous findings from Martinez Sanz et al. [22] who demonstrated that unmodified cellulose nanowhiskers should be handled in a partially hydrated state

instead of freeze-dried, as it is very difficult to re-disperse them due to the strong hydrogen bonding and subsequent self-association. However, only slight improvements in mechanical properties were obtained and no barrier properties were reported for this melt extruded CNW-containing nanocomposites. Poor compatibility between highly hydrophilic cellulose nanowhiskers and the hydrophobic PHBV in the melt state was observed by Jiang et al [10] which complicated the filler dispersion and gave rise to weak polymer-nanofiller interactions. They observed that, despite using polyethylene glycol as a compatibilizer, cellulose nanowhiskers agglomerated during freeze-drying and could not be broken and well-dispersed by the extrusion process. Using the previously mentioned technique of creating an initial masterbatch prior to the melt mixing step, Srithep et al. [23] incorporated nanofibrilated cellulose (NFC) into PHBV. Improvements in Young´s Modulus (90%) and in storage modulus (137%) were obtained for the materials with 10 wt.% of NFC. However, even though individual fibers were observed, some NFC agglomerates were still distinguished. Moreover, NFC triggered the PHBV degradation at high processing temperatures, thus precluding its use in processes such as melt compounding.

Ball milling technique is an efficient and green strategy, constituting another alternative to develop composites. It is considered a novel compounding method being previouslly used in the development of clay, layered double hydroxide or carbon-based nanocomposites [24-32]. Moreover, it has also been used for polymer nanocomposites where there was low compatibility between filler and matrix aiming to overcome the lack of affinity between both components [25]. However, there is scarce literature reporting on the use of ball milling to generate cellulose-based nanocomposites. Moreira et al. [33] dispersed cellulose nanowhiskers in starch-based thermoplastics using solid state ball milling. Nanowhiskers agglomeration was minimized using a

polysaccharide as a coating in a previous step and a reinforcing effect was noticed with improvements in Young's modulus from 29 to 132 MPa and tensile strength from 1.8 to 4.9 MPa. In addition, high energy ball milling has also been used to incorporate BCNW into PLA without the need of any previous nanofiller treatment [34]. Increased mechanical and oxygen barrier properties up to 10% (in Young's Modulus and tensile strength) and 18%, respectively, were obtained.

This work describes the preparation of nanocomposites using BCNW as a filler via the ball-milling technique. The main objetive was to evaluate the potential of this easy, one single step and "green" technique to produce PHBV/BCNW nanocomposites with improved properties. Thermal properties, thermal stability, morphology, mechanical and barrier properties of the developed nanocomposites were studied.

2. MATERIALS AND METHODS

2.1 Materials

Poly (hydroxybutyrate-co-valerate) (PHBV) was supplied by Goodfellow Cambrigde Limited (Hurtingdon, England). This grade consisted of a PHBV copolymer containing 12% mol of hydroxyvalerate plasticized with citric ester. Prior to the ball milling process, the material was purified by dissolution in $CHCl_3$ and subsequently precipitated by drop-wise addition to an excess of methanol. The material, in this way, was transformed from pellet to powder form which was necessary for the ball milling process. Sulphuric acid 96 wt.% and sodium hydroxide pellets were purchased from Panreac (Barcelona, Spain). The bacteria strain *Gluconacetobacter xylinus* was obtained from the Spanish type culture collection (CECT).

2.2 Preparation of bacterial cellulose mats

The bacteria *Gluconacetobacter xylinus* was incubated in a modified Hestrin/Schramm medium at 30 ºC [22]. All of the cells were pre-cultured in a test tube containing 5 mL of media. When a thin layer of cellulose was detected on the surface, they were transferred to 200 mL bottles and, subsequently, to a bigger reactor of 20 L. The synthesized bacterial cellulose pellicles, of about 2 cm thickness obtained thereof were cut up (ca. 2cm×2cm), sterilized and cleaned in boiling water and in a 10 wt.% (v/v) NaOH aqueous solution to remove bacterial cells and absorbed culture media. Finally, the pH was adjusted to neutral by boiling in distilled water several times.

2.3 Preparation of bacterial cellulose nanowhiskers (BCNW)

BCNW were obtained by the optimized method reported by Martínez-Sanz et al. [35]. Briefly, small pieces of bacterial cellulose at neutral pH were ground in a blender. A gel-like material was obtained and compressed in order to remove most of the absorbed water. The partially dried cellulosic material was then treated with 301 mL sulfuric acid/L water, in a cellulose/acid ratio of approximately 7 g/L, at 50 ºC for three days, until a homogenous solution was obtained. The cellulose nanowhiskers were obtained as a white precipitate after several centrifugations and washing cycles at 12.500 rpm and 15 ºC for 20 min. The pH of the samples was measured after the washing-centrifugation cycles, being around 2 for all the samples. Then, the material was re-suspended in deionized water and neutralized with sodium hydroxide until neutral pH and, subsequently, centrifuged to obtain BCNW as a partially hydrated precipitate. Finally, the material was freeze dried and ground prior to its use in the ball milling process.

2.4. Preparation of PHBV/BCNW nanocomposites

Ground BCNW and PHBV powders were milled in the solid state in a Retsch (Germany) centrifugal ball mill (model PM100). The milling process was carried out in a cylindrical steel jar of 50 cm^3 with 5 steel balls of 10 mm of diameter. The rotation speed used was 650 rpm and the milling time was fixed at 60 min. In these experimental conditions, three series of composites PHBV/BCNW with 0.5, 1 and 3 wt.% of BCNW were prepared. An additional PHBV sample without nanofiller to be used as a reference was also milled in the same conditions. The PHBV/BCNW mixtures and the pure milled PHBV were moulded in a hot press (Carver Inc.) at 170 ºC and cooled at room temperature forming 250 ± 50 µm thick films.

2.5. Characterization of the nanocomposites

2.5.1. Optical properties of the films

The opacity of the films was measured by using a Konica Minolta CM-2500d X-Rite SP60 Series spectrophotometer following the ASTM E284 ("Terminology of Appearance"). The opacity was defined as ability of a thin film to hide a surface behind and in contact with it, expressed as the ratio of the reflectance factor (R_b) when the material is backed by a black surface to the reflectance factor (R_w) when it is backed by a white surface (usually having a reflectance factor of 0.89). The opacity (O) was calculated using the relationship: O (%) = (R_b/R_w) x 100.

2.5.2. Scanning Electron Microscopy (SEM).

The microstructural analysis of the PHBV/BCNW nanocomposites was carried out by SEM using a scanning electron microscope (Hitachi S4100). Samples were frozen in liquid nitrogen and cryo-fractured to observe the cross-section of the nanocomposites.

The samples were mounted on bevel sample holders, sputtered with Au/Pd under vacuum and observed using an accelerating voltage of 10 kV.

2.5.3. Transmission Electron Microscopy (TEM)

Transmission electron microscopy (TEM) was performed using a JEOL 1010 (Jeol, Tokyo, Japan) equipped with a digital Bioscan (Gatan) image acquisition system. TEM observations were performed on ultrathin sections of microtomed thin composite sheets.

2.5.4. Differential Scanning Calorimetry (DSC)

Differential scanning calorimetry (DSC) analysis was carried out, in duplicate, on 10-12 mg of dry samples at a heating rate of 10 ºC min^{-1} from 0ºC to 180 ºC in a nitrogen atmosphere by means of a DTA Mettler Toledo (DSC 30). The first and second melting endotherms, after controlled crystallization at 10 ºC min^{-1} from the melt, were analysed. The crystallinity (%) was estimated from the corrected enthalpy for biopolymer content in the samples, following the equation (1).

$$\%Xc = \frac{\Delta H_f}{\Delta H_f^o (1-w)} \times 100 \quad (1)$$

where ΔH_f is the enthalpy of fusion of the studied specimen, ΔH^o_f is the enthalpy of fusion of a totally crystalline material and w is the weight fraction of the filler. The ΔH^o_f used for this equation was 109 J g^{-1} for PHBV [36, 37].

In addition, an isothermal crystallization kinetics study was performed as follows: The samples were heated from room temperature to 180 ºC at 75 ºC $min^{-1}$and held for 10 min to erase the thermal history. Then, they were cooled rapidly, at 100 ºC min^{-1}, to the desired crystallization temperatures (in this case 133, 135 and 137 ºC), ensuring that the crystallization process did not start during the cooling step. After that, the temperature

was held until the crystallization process was completed and, finally, the samples were heated at 10 ºC min^{-1} to 180 ºC again to obtain the melting temperature.

2.5.5. X-ray Diffraction

X-ray diffraction (XRD) measurements were performed with a Brucker diffractometer (equipped with a continuous scan attachment and a proportional counter) with Ni-filtered Cu Kα radiation (λ= 1.54050 Å). The samples were examined over the angular range of 2º to 40º with a step size of 0.03º and a count time of 0.2 s per point.
Peak fitting was carried out using Igor software package (Wavemetrics, Lake Oswego, Oregon). Gaussian function was used to fit the experimental diffraction profiles obtained. For the fitting procedure, the reflections considered were eight at 13.4º, 16.8º, 19.8º, 21.4º, 22.3º, 25.5º, 27.0º and 30.0º 2θ (corresponding to the 020, 110, 021, 101, 111, 121, 040 and 002 crystal planes, respectively) assigned to the crystalline part of the semicrystalline PHBV and one assigned to the amorphous halo centred at ~16º 2θ. The crystallinity index $CI\ (X_i)$ was determined by the method reported by Martínez Sanz et al. [22].

$$CI(X_i) = \frac{\sum A_{Crystal}}{\sum A_{Total}} x100 \quad (2)$$

Where ΣA_{Total} is the sum of the areas under all the diffraction peaks and $\Sigma A_{Crystal}$ is the sum of the areas corresponding to crystalline peaks.

2.5.6. Thermogravimetric analysis (TGA)

Thermogravimetric (TG) curves were recorded using a Mettler TC-10 thermobalance. The samples (~5 mg) were heated from 25°C to 800 °C at a heating rate of 10 ºC min^{-1}

under air and nitrogen atmosphere. Derivate thermogravimetric curves (DTG) express the weight loss rate as a function of temperature.

2.5.7. Dynamic Mechanical Analysis (DMA)

Mechanical properties were evaluated using a DMA TAQ800. Measurements were conducted at constant frequency (1Hz) and amplitude (5µm). The temperature was varied between -30°C and 140°C at 3°C min^{-1}.

2.5.8. Mass transport properties.

The oxygen transmission rate of the various samples was determined at 80% relative humidity (RH) and 25 ºC using an Oxtran 100 equipment (Modern Control Inc., Minneapolis, MN, USA). 80% RH was generated by a built-in gas bubbler and was checked with a hygrometer placed at the exit of the detector. Samples were purged with nitrogen for a minimum of 20 h in the previously relative humidity equilibrated samples, prior to exposure to an oxygen flow of 10 mL min^{-1}. The exposure area during the test was 5 cm^2 for each sample. In order to obtain the oxygen permeability, film thickness and gas partial pressure were considered in each case.

Water sorption was measured on different strips of the sample by subjecting the samples to a 100% relative humidity conditions at 25°C. The weight uptake was followed as a function of time. Equilibrium sorption was assumed when no further weight changes were observed. The data were averaged on at least two samples. Since all the samples analysed showed Fickian behaviour, i.e. a linear dependence of water sorption with the square root of time, it was possible to derive the mean diffusion coefficient D ($cm^2\ s^{-1}$) from the linear part of the reduced sorption curve:

$$\frac{C_t}{C_{eq}} = \left(\frac{16D}{\pi l^2}\right)^{1/2} t^{1/2} \quad (3)$$

where l is the thickness of the sample, C_t is the penetrant concentration at the time t, and C_{eq} is the penetrant concentration at the equilibrium value.

2.5.9. Statistical analysis

Some of the results were analysed by multifactor analysis of variance (ANOVA) using Statgraphics Centurion 15.1 software (Statpoint Technologies, INC, Warrenton, VA, USA). Tukey's test was used at the 95% confidence level.

3. RESULTS AND DISCUSSION

3.1. Morphology and optical properties of the PHBV/BCNW nanocomposites obtained by ball-milling

Bacterial cellulose nanowhiskers (BCNW) were successfully obtained with average cross-sections of ~22 nm and length of ~600 nm, as previously reported [19]. To study the dispersion of the BCNW within the PHBV matrix, the cryo-fractured surface of nanocomposite films were examined by SEM (cf. Figure 1). For the nanocomposite films, the figures correspond to the areas were some agglomerates were detected. SEM images of the samples confirmed that BCNW were agglomerated within the nanocomposites, even for the sample with the lowest nanofiller content, and a lack of interfacial interaction between the polymer matrix and the BCNW agglomerates was apparent. This could be attributed, not only to the discrete compatibility between the hydrophilic nanofiller and PHBV, but also to the fact that the BCNW were added as a freeze-dried product with strong hydrogen bonding self-association which could not be

disrupted even with the intense mechanical treatment applied during ball milling. Moreover, increasing the nanocellulose content up to 1 or 3 wt.% in the materials resulted in bigger aggregates, as observed from the SEM images. In spite of that, from the TEM micrographs shown in Figure 2, it can be observed that a significant fraction of the filler was properly dispersed and distributed at the nanoscale level, even though the previously mentioned aggregates were also present in the TEM images. Therefore, although a complete dispersion of the nanofiller could not be attained through ball milling, a fraction of the added BCNW was properly dispersed and distributed within the polymeric matrix as a result of the processing step.

Figure 3 shows the contact transparency images of the nanocomposite films with different BCNW loadings. It was observed that the nanocellulose aggregates present in the nanocomposites did not significantly affect the optical properties at the macroscopic level. Moreover, optical properties were measured by a quantitative method. Thus, opacity values are presented in Table I. From this table it can be observed no effect on the apparent opacity after BCNW addition. In fact, contrary to expectation, the addition of the highest content of BCNW did not lead to an increase of the opacity, but rather the opposite. These results are in accordance with previous work incorporating BCNW by the same technique showing almost no effect on the apparent opacity of the materials after BCNW addition [34]. In this case, higher opacity for PHBV was observed if compare with the above mentioned work [34], mainly due to the fact that PHBV is a relatively opaque material compared with PLA. Thus, the nanocomposite films obtained after compression moulding of the different formulations obtained through ball milling were optically identical to the neat PHBV film, indicating that the transparency of the pure PHBV was kept for all the specimens developed.

3.2 FTIR study of PHBV/BCNW nanocomposites

Figure 4 illustrates FTIR spectra of the nanocomposites. Characteristic peaks from both PHBV and BCNW were present in the FTIR spectra of the nanocomposites. For instance, the broad bands at 3400 cm^{-1} and 2900 cm^{-1} were assigned to O-H stretching vibration and C-H stretching vibrations modes of BCNW, respectively [16,38,39]. Bands at 3436 and 3342 cm^{-1} have been typically ascribed to free and hydrogen bonded O-H stretching vibrations, respectively [11,16,39]. From Figure 4, it can be observed that upon increasing the BCNW content, the intensity of the broad band at 3400 cm^{-1} increased and the band related to the hydrogen bonded O-H stretching vibrations was more noticeable. This result suggests that although a chemical grafting between the hydroxyl groups from BCNW and the reactive groups from the PHBV did not occur, hydrogen bonds could be generated within the nanocomposites between hydroxyl groups from BCNW surface and carbonyl groups present in the PHBV. An increase and sharpening of the previously reported bands associated to hydrogen bonded carbonyl groups at around 1723 cm^{-1} [16,39,40] can be also observed in Figure 4 which further confirms the interaction between both components. Moreover, it has been demonstrated that this band is sensitive to the PHBV crystallinity [41] and, thus, the observed increase in the intensity of this band upon increasing BCNW content could also be related to an increase in the polymer crystallinity. In order to quantitatively corroborate this increase, a normalization of the band at 1723 cm^{-1} was performed using the ratio of the intensities at 1723 cm^{-1} and 1750 cm^{-1}. The obtained values for this ratio were 1.03, 1.04, 1.07 and 1.10 for pure PHBV and samples with 0.5, 1 and 3% BCNW loading respectively. It confirms the increase of this band after BCNW addition. This observation can be supported by the increase in the FTIR band located at 1381 cm^{-1}, which is also known to be sensitive to changes in PHBV crystallization [15].

3.3 Thermal properties and thermal stability of PHBV/BCNW nanocomposites

The degree of crystallinity plays an important role in the physical properties and biodegradability of polymers. Thermal properties of neat PHBV and the nanocomposite materials were evaluated by means of DSC analyses. The melting temperature (T_m) and heat of fusion (ΔH_m) were determined from the first and second heating runs. The degree of crystallinity (X_c) of the specimens was determined from the first heating run curve, offering information related to the thermal characteristics of the just obtained material. Crystallization temperature (T_c) and enthalpy (ΔH_c) values were also obtained from the cooling run. Table II shows the thermal parameters of the neat PHBV and the BCNW-containing nanocomposites.

As shown in Figure 5a, the DSC traces of the first heating scan showed two melting peaks, which have been previously reported [6,42] and interpreted as an effect of the melting-recrystallization process occurring during subsequent heating [43]. During the slow heating scans, unstable crystals have sufficient time to melt and reorganize into more stable crystals which lead to this bimodal melting peak behaviour. The reorganized crystals are subsequently re-melted at higher temperatures [44,45]. Moreover, Wang et al. [46] observed the same bimodal effect in PHBV/clays nanocomposites with an increase in the high-temperature melting peak area upon addition of clays. They pointed out that the low-temperature melting peak was probably related to homogeneous nucleation of PHBV which started spontaneously by PHBV chain aggregation below the melting point. On the contrary, the high-temperature melting peak was related to heterogeneous nucleation of PHBV, and its increase was associated to the existence of much more crystalline nuclei after addition of clays than in neat PHBV [46]. DSC results showed that while for lower loadings there was no effect in the low melting peak temperature, addition of greater amounts of BCNW up to

3 wt.% decreased the lower melting peak temperature ca. 5 ºC, when compared with the neat PHBV. Nevertheless, although at high loadings the fraction of crystals that melted at low temperature was composed by smaller or more defective crystals, its proportion was substantially reduced as could be discerned from the area ratio of both melting peaks areas, hence reducing its contribution to the total enthalpy of the material (cf. Figure 5a.). In fact, an increase in the area and height of the second melting peak related to the first melting peak was observed with increasing BCNW content. Moreover, a sharpening of the high temperature melting peak was also observed. From all the previous observations it could be stated that at higher loadings the fraction of crystals which melted at higher temperature (heterogeneous crystallization) increased, being in accordance with the observations of Wang et al. [46] and, hence, suggesting that BCNW could act as nucleating agents. These results were similar to those observed by Jiang et al. [10] who reported an enhancement of the crystallization ability upon addition of CNW into PHBV, but different from those reported by Martínez-Sanz et al. [6]who suggested that the CNW somehow hindered the crystallization process of PHBV. Both studies were carried out with cellulose-based nanocomposites obtained by solution casting with the same PHBV grade as the one used in this study. Therefore, the addition of BCNW affected the heterogeneous and homogeneous crystallization of the PHBV with a clear promotion of the heterogeneous crystallization process. As shown in Table II, the melting enthalpy values increased with BCNW addition, indicating an increase in the crystallinity, mainly for higher BCNW loadings. As already mentioned, this could be ascribed to a nucleating effect exerted by the well dispersed and distributed fraction of the BCNW. These results are well correlated with the previous FTIR observations. In fact, it is well established that nanowhiskers and other nanofillers in nanocomposites may act as nucleating sites and, thus, affect the crystallization kinetics of the polymeric

matrix. An exothermic peak was observed for all specimens during the cooling scan which corresponded to the crystallization of PHBV (Figure 5b). Although there were no great differences in the crystallization temperature, increased crystallization enthalpies were observed when BCNW were added, particularly at high concentrations. This again confirmed the nucleation ability of the nanowhiskers. After erasing the thermal history of the materials, only one melting peak was observed in the thermograms (cf. Figure 5c) and the melting temperature values ranged between those obtained in the first and second melting peaks from the first heating run. It should be mentioned that while melting temperature was almost unaltered with the addition of BCNW, an increase in the melting enthalpy and a sharpening of the melting peaks were observed for the nanocomposite materials (cf. Table II and Figure 5c).

The thermal stability of the neat PHBV and PHBV/BCNW nanocomposite samples were examined using TGA. Figure 6 shows TG and DTG curves under air and nitrogen environments. The temperatures corresponding to the onset of decomposition (T_{onset}) are essential for evaluating the thermal stability of the nanocomposites and are reported in Table III. It is widely known that cellulose nanowhiskers obtained by acid hydrolysis using sulfuric acid lead to sulfate groups grafted on CNW surface with a negative effect of their thermal stability [47]. On the contrary, as above commented, an optimized method to perform the BCNW was used in this work [35] which demonstrated that, even using a sulfuric acid in the hydrolysis process, a neutralization step after hydrolysis led to an increase of the thermal stability of BCNW in regard to pristine bacterial cellulose. Moreover, several studies reported that cellulose nanowhiskers were able to improve the thermal stability of the PHBV [11,15,16,39], while a slight decrease on thermal degradation was observed in other cases [9]. Thermal degradation through a one-step process was observed in both environments, although a small shoulder was

observed around 320-350 ºC. Under inert atmosphere the thermal stability of the nanocomposites was better than that for the neat PHBV but worse than that for the pure BCNW. It fact, it was found that with the increase in BCNW contents, the degradation temperature (T_d) increased from 276.0 ºC for the neat PHBV to 284.8 ºC for the nanocomposite film with 0.5 wt.%, showing at this concentration the maximum improvement, and then decreased slightly to 282.2 ºC for 3 wt.% BCNW. Similar behaviour has been recently reported with a maximum improvement at low loading levels above which the degradation temperature was decreased [14]. It is widely recognized that the general mechanism of thermal degradation of PHBV is the scission of PHBV molecules by a random cis-elimination reaction at a six-membered ring ester intermediate which take place at the initial steps of PHBV decomposition. It has been observed that addition of CNW suppressed the formation of this intermediate due to the strong hydrogen bonds interactions [39]. However, once the maximum degradation temperature was reached, the degradation process was accelerated due to the increased thermal conductivity of the CNW [39]. As observed in the morphological analysis, more agglomerates were noticed at high BCNW addition. This implies a reduction of the hydroxyl groups from BCNW surface available to form hydrogen bonds with the PHBV matrix, thereby reducing the thermal stability to some extent at those loading levels. However, results obtained in air conditions showed a different trend. While for 0.5 wt.% a slight improvement in thermal stability was detected, higher loadings led to a decrease in degradation temperature, probably due to the fact that oxidative degradation took place in this atmosphere. Therefore, it can be stated that nanocomposites containing BCNW behaved differently depending on the environmental conditions, i.e. oxidative thermal degradation of the PHBV or thermal degradation by pyrolysis. Regarding the small shoulder observed in both air and nitrogen environments and taking

in account the degradation curve of the pure BCNW, the mass loss could be attributed to the degradation of BCNW present in the nanocomposite. In fact, the higher the BCNW concentration, the larger the weight loss observed at this point. Results also showed that addition of BCNW increased the residual content at 600 ºC of the PHBV/BCNW nanocomposites, indicating that a higher fraction of the material did not volatilize upon thermal degradation.

3.4 Thermo-mechanical properties of PHBV and its nanocomposites.

The thermo-mechanical properties of neat PHBV and its nanocomposites prepared with BCNW were also investigated using dynamo mechanical analysis (DMA). DMA can also be used to determine how the mechanical properties of specimens vary with temperature. The resulting storage modulus and tanδ relaxation temperature of neat PHBV and PHBV/BCNW nanocomposites are shown in Figure 7 and 8, respectively. Glass transition temperature (T_g) values could not be discerned by DSC, but they can be obtained through DMA. Figure 8 shows that tanδ relaxation of PHBV increased with BCNW addition, which can be caused by the restriction of the chain mobility within the polymer matrix after nanofiller incorporation. The neat PHBV exhibited a tanδ transition around 16 ºC, which could corresponds to the T_g of the PHB [48] and it increased with the increase in BCNW content. The results also showed that the nanofiller increased the storage modulus of the neat PHBV at temperatures below the tanδ relaxation temperature (Figure 7). The increase in the storage modulus can be ascribed to the reinforcing effect of the nanofillers. Similar effects were observed in PHBV-based nanocomposites with CNW [10] or carbon nanotubes [49].

3.4 Crystal structure and crystallinity of PHBV/BCNW nanocomposites

Crystal structures of the neat PHBV and PHBV/BCNW nanocomposites were studied by X-ray diffraction. The diffraction patterns are shown in Figure 9 and the crystal parameters and polymer crystallinity index (X_i) were calculated and are summarized in Table IV. The diffractogram of the neat PHBV shows that this biopolyester is a semicrystalline material. Nanocomposites containing BCNW showed PHBV reflections at the same values as the neat biopolymer, indicating that, in the nanocomposites, PHBV crystallized in its typical orthorhombic crystalline form [49-51]. In fact, the same interplanar distances were obtained for PHBV and its nanocomposites using Bragg´s law (cf. Table IV) defined by the following equation.

$$n\lambda = 2d\sin\theta \quad (4)$$

where n is an integer, λ is the wavelength of incident wave, d is the interplanar spacing, and θ is the angle between the incident ray and the scattering planes. The results suggest that the parameters of PHBV unit cell were not influenced by BCNW addition. However, as shown in Figure 9, sharper and more intense peaks can be discerned for the (020) plane upon BCNW addition, which is related with the crystallite size that was determined using the well-known Scherrer equation (equation 5) [49]:

$$L(nm) = \frac{K\cdot\lambda}{\beta\cdot\cos\theta} \quad (5)$$

where L is the crystallite size (nm), K is a dimensionless shape factor with a value close to unity, which is K=0.94 for an orthorhombic cell [49], λ is the wavelength of the X-ray radiation which for CuKα radiation is 1.54Å, θ is the Bragg angle and β is the full width half maximum (FWHM). Table IV shows an increase in the crystal lamella size in the direction normal to the (020) plane with increasing BCNW content. Crystallinity values were also obtained from PHBV and its nanocomposite diffractograms. It is worth noting that the data calculated from the diffractograms were in very good agreement with those calculated by DSC. As observed before, an increase in the crystallinity took

place after BCNW addition. Once again, these results confirm that higher crystalline fraction was obtained in PHBV/BCNW nanocomposites. In line with the above, it is has been reported that CNW could affect the crystallization of PHBV in two opposite ways. CNW can act as nucleating agent increasing the nucleation and, hence, the overall crystallization rate, thus leading to more perfect crystals, but, on the contrary, when strong interactions take place between CNW and PHBV, the mobility of PHBV chains become more limited and hence crystallinity decreases [40]. Thus, attending to the morphological analysis performed here, due to the existence of some agglomerates, the hydroxyl groups from BCNW surface were reduced, hence reducing the BCNW-PHBV interactions. Because of that, polymer chains could easily move generating an increment in the polymer crystallinity, as observed by DSC and X-ray diffraction.

3.5 Isothermal crystallization of PHBV/BCNW nanocomposites

Isothermal crystallization of neat PHBV and PHBV/BCNW nanocomposites was investigated at three crystallization temperatures 133, 135 and 137 ºC. The crystallization kinetics of neat PHBV and PHBV/BCNW nanocomposites under isothermal crystallization conditions were analysed by the Avrami equation (6) [52-54].

$$X(t) = 1 - \exp\left(-kt^n\right) \quad (6)$$

where $X(t)$ is the relative crystallinity at time t, k is the overall crystallization rate constant and n is the Avrami index, which depends on the type of nucleation and the geometry of growing crystals. The derivative method reported by De Santis and Pantani [55] was used to directly fit the calorimetric curve of the isothermal crystallization process to the derivative form of the Avrami equation. Figure 10 shows, as an example, the DSC curves for PHBV/BCNW 1 wt.% nanocomposites obtained at the different isothermal crystallization temperatures, with the corresponding Avrami fittings. The

data obtained from the plots corresponding to Avrami kinetic parameters are listed in Table V.The half-time of crystallization ($t_{½}$) is defined as the time needed to reach 50% crystallization. It is also used to directly characterize the crystallization rate, since the reciprocal half-time of crystallization ($1/ t_{½}$) can be considered approximately proportional to the crystal growth rate [56]. Thus, it can be said that the shorter the half-time of crystallization, the higher the crystallization rate. In view of the results, although a slight increment in the *K* parameter was observed, $t_{½}$ was, in general, clearly reduced for all nanocomposites, indicating that the presence of BCNW facilitated the crystallization process. This effect is in agreement with the above mentioned non-isothermal crystallization study performed by DSC.

3.6 Mass transport properties

Oxygen permeability (OP) of PHBV and PHBV/BCNW nanocomposites was measured at 80% RH and the results are gathered in Table VI. The permeability value of neat PHBV obtained through ball milling was lower to that reported in the literature for PHBV films obtained through melt compounding or solution casting [6,57]. One of the factors that could explain this effect is the higher crystallinity obtained for the neat PHBV processed by ball milling, which was almost double than the crystallinity reported in those studies, as crystalline domains are considered impermeable to low molecular weight molecules increasing the tortuosity [5,16]. In fact, this oxygen permeability value was found to be close to that of similarly processed PHBV which also reached similar values in crystallinity, as reported in a previous work [58]. Moreover, oxygen barrier properties improved upon addition of BCNW, as can be seen in Table VI, suggesting that the dispersed fraction of crystalline nanofillers partially blocked the oxygen diffusion. A maximum oxygen permeability drop of ca. 22% was attained for the samples with 0.5 wt.% of BCNW. To the best of our knowledge, this is

the largest oxygen permeability reduction reported for PHBV nanocomposites loaded with BCNW up to date. This reduction in the oxygen permeability values highlights the oxygen barrier properties of the so-obtained PHBV/BCNW nanocomposites demonstrating the blocking capacity of BCNW. Increasing the BCNW content, i.e. for 1 and 3 wt.%, did not result in further improvements on barrier properties, but it did not grow worse. This reduction in oxygen permeability could be also related to the further increase on crystallinity degree of the polymeric matrices upon addition of BCNW as observed by DSC, which could lead to a greater tortuosity as mentioned above. At high contents a balance between tortuosity due to the blocking effect created by addition of well dispersed fillers [14,16] and filler agglomeration of the BCNW creating preferential paths could take place since although greater improvements could be expected upon addition of higher amounts of BCNW, the presence of higher agglomerates at those loading levels generated preferential paths to the permeant pass through. Similar results were obtained after incorporation of BCNW into PLA by ball milling where the best result was also obtained for the lowest loading, 0.5.wt%, as in this case. Higher loading of BCNW did not result in further improvements of the oxygen permeability [34]. Moreover, although addition of low amounts of BCNW into polymeric matrices such as PLA by melt mixing resulted in a reduction of the oxygen permeability measured at high relative humidity, an increase of the BCNW loading led to a detrimental effect in the oxygen barrier performance [13]. These effects was mainly due to the presence of filler agglomerates at high contents highlighting the importance of dispersion to optimize the performance improvements in this kind of films.

Water vapour sorption and diffusion were also measured, and the data are reported in Table VII. Although no statistically significant differences were noticed for the water vapour sorption of the various samples, an increasing tendency was observed when

incorporating BCNW, mainly due as a consequence of the presence of hydroxyl groups on cellulose surface. This result was in accordance with previous results incorporating different kinds of CNW, including BCNW, into PHBV where although a trend of increased water uptake was observed, there were not statistically significant differences upon filler addition [6]. Moreover, a reduction in the diffusion coefficients was generally observed. In agreement with the oxygen permeability measurements, apart from the blocking effect exerted by BNCW, the crystallinity degree was closely related with these results. However, for loadings of 3 wt.%, no further improvements were observed for the diffusion coefficient, probably due to the presence of more frequent and bigger agglomerates, as observed by microscopic analysis, which was also in accordance with the observations in the oxygen permeability study. In any case, this coefficient remained below the values of the unfilled polymer.

4. CONCLUSIONS

In this work, PHBV nanocomposite films loaded with bacterial cellulose nanowhiskers (BCNW) were produced by the potentially environmentally friendly technique of ball-milling and the effects of cellulose nanowhiskers loading in the morphology, thermal properties and stability, isothermal crystallization, dynamo-mechanical properties and barrier properties were studied. Morphological evaluation clearly revealed a relative good dispersion and distribution of the BCNW within the polymeric matrix although some BCNW aggregates remained present in the nanocomposites after the ball milling process. The results confirmed that the well dispersed fraction of BNCW acted as nucleating agents and their addition favored the crystallization phenomena of the PHBV, which was corroborated by the isothermal crystallization study. Thermal stability of the PHBV was improved by addition of BCNW when measured under inert

atmosphere but, on the contrary, under air conditions, only the nanocomposite with 0.5 wt.% BCNW showed an improvement. Regarding the barrier properties, the oxygen permeability was improved up to 22% after the addition of 0.5 wt.% of BCNW. A reduction of the water vapour diffusion coefficient was also obtained. Although some BCNW aggregates were present after the ball milling process, in general, this processing method resulted in materials with improved thermal stability, crystallinity, oxygen barrier properties and reduced water vapour diffusion coefficient, showing its potential for nanocomposite development.

Acknowledgments

J Ambrosio-Martín would like to thank the Spanish Ministry of Economy and Competitiveness for the FPI grant BES-2010-038203. M.J. Fabra is recipient of a "Juan de la Cierva" contract from the Spanish Ministry of Economy and Competitiveness. The authors acknowledge financial support from the MINECO (MAT2012-38947-C02-01 project) and from the FP7 ECOBIOCAP project.

REFERENCES

1. J. Gonzalez-Lopez; C. Pozo; M. V. Martinez-Toledo; B. Rodelas; V. Salmeron, International Biodeterioration and Biodegradation 38(1996) 271.
2. M. Lai; J. Li; J. Yang; J. Liu; X. Tong; H. Cheng, Polym Int 53(2004) 1479.

3. G. X. Chen; G. J. Hao; T. Y. Guo; M. D. Song; B. H. Zhang, J Appl Polym Sci 93(2004) 655.
4. F. Ublekov; J. Baldrian; E. Nedkov, J Polym Sci, Part B: Polym Phys 47(2009) 751.
5. M. D. Sanchez-Garcia; J. M. Lagaron, J Appl Polym Sci 118(2010) 188.
6. M. Martínez-Sanz; A. A. Vicente; N. Gontard; A. Lopez-Rubio; J. M. Lagaron, Cellulose (2014)
7. I. Kvien; J. Sugiyama; M. Votrubec; K. Oksman, J Mater Sci 42(2007) 8163.
8. L. Petersson; I. Kvien; K. Oksman, Composites Science and Technology 67(2007) 2535.
9. E. Ten; J. Turtle; D. Bahr; L. Jiang; M. Wolcott, Polymer 51(2010) 2652.
10. L. Jiang; E. Morelius; J. Zhang; M. Wolcott; J. Holbery, Journal of Composite Materials 42(2008) 2629.
11. H. Y. Yu; Z. Y. Qin; L. Liu; X. G. Yang; Y. Zhou; J. M. Yao, Composites Science and Technology 87(2013) 22.
12. E. Ten; L. Jiang; M. P. Wolcott, Carbohydr Polym 90(2012) 541.
13. M. Martínez-Sanz; A. Lopez-Rubio; J. M. Lagaron, Biomacromolecules 13(2012) 3887.
14. M. Martínez-Sanz; M. Villano; C. Oliveira; M. G. E. Albuquerque; M. Majone; M. Reis; A. Lopez-Rubio; J. M. Lagaron, New Biotechnol 31(2014) 364.
15. H. Y. Yu; Z. Y. Qin; C. F. Yan; J. M. Yao, ACS Sustainable Chemistry and Engineering 2(2014) 875.
16. H. Yu; C. Yan; J. Yao, RSC Advances 4(2014) 59792.
17. A. Arias; M. C. Heuzey; M. A. Huneault; G. Ausias; A. Bendahou, Cellulose (2014)

18. M. Martínez-Sanz; A. Lopez-Rubio; J. M. Lagaron, J Appl Polym Sci 128(2013) 2666.
19. J. Ambrosio-Martín; M. J. Fabra; A. Lopez-Rubio; J. M. Lagaron, Cellulose 22(2015) 1201.
20. A. L. Goffin; J. M. Raquez; E. Duquesne; G. Siqueira; Y. Habibi; A. Dufresne; P. Dubois, Biomacromolecules 12(2011) 2456.
21. N. Herrera; A. P. Mathew; K. Oksman, Composites Science and Technology 106(2015) 149.
22. M. Martínez-Sanz; R. T. Olsson; A. Lopez-Rubio; J. M. Lagaron, Cellulose 18(2011) 335.
23. Y. Srithep; T. Ellingham; J. Peng; R. Sabo; C. Clemons; L. S. Turng; S. Pilla, Polym Degrad Stab 98(2013) 1439.
24. L. Vertuccio; G. Gorrasi; A. Sorrentino; V. Vittoria, Carbohydr Polym 75(2009) 172.
25. F. Perrin-Sarazin; M. Sepehr; S. Bouaricha; J. Denault, Polym Eng Sci 49(2009) 651.
26. V. Bugatti; G. Gorrasi; F. Montanari; M. Nocchetti; L. Tammaro; V. Vittoria, Appl Clay Sci 52(2011) 34.
27. L. Tammaro; V. Vittoria; V. Bugatti, Eur Polym J 52(2014) 172.
28. G. Gorrasi; V. Bugatti; V. Vittoria, Carbohydr Polym 89(2012) 132.
29. G. Gorrasi; M. Sarno; A. Di Bartolomeo; D. Sannino; P. Ciambelli; V. Vittoria, J Polym Sci, Part B: Polym Phys 45(2007) 597.
30. G. Gorrasi; E. Piperopoulos; M. Lanza; C. Milone, J Phys Chem Solids 74(2013) 1.
31. G. Gorrasi; R. Di Lieto; G. Patimo; S. De Pasquale; A. Sorrentino, Polymer 52(2011) 1124.

32. H. Wu; W. Zhao; G. Chen, J Appl Polym Sci 125(2012) 3899.

33. F. K. V. Moreira; J. M. Marconcini; L. H. C. Mattoso, Cellulose 19(2012) 2049.

34. J. Ambrosio-Martín; A. Lopez-Rubio; M. J. Fabra; G. Gorrasi; R. Pantani; J. M. Lagaron, J Appl Polym Sci 132(2014) 41605.

35. M. Martínez-Sanz; A. Lopez-Rubio; J. M. Lagaron, Carbohydr Polym 85(2011) 228.

36. A. Buzarovska; G. Bogoeva-Gaceva; A. Grozdanov; M. Avella; G. Gentile; M. Errico, J Mater Sci 42(2007) 6501.

37. M. Scandola; M. L. Focarete; G. Adamus; W. Sikorska; I. Baranowska; S. Świerczek; M. Gnatowski; M. Kowalczuk; Z. Jedliński, Macromolecules 30(1997) 2568.

38. G. Chen; A. Dufresne; J. Huang; P. R. Chang, Macromol Mater Eng 294(2009) 59.

39. H. Y. Yu; Z. Y. Qin; Y. N. Liu; L. Chen; N. Liu; Z. Zhou, Carbohydr Polym 89(2012) 971.

40. H. Y. Yu; J. M. Yao; Z. Y. Qin; L. Liu; X. G. Yang, J Appl Polym Sci 130(2013) 4299.

41. B. Fei; C. Chen; H. Wu; S. Peng; X. Wang; L. Dong, Eur Polym J 39(2003) 1939.

42. M. D. Sanchez-Garcia; E. Gimenez; J. M. Lagaron, Carbohydr Polym 71(2008) 235.

43. L. M. W. K. Gunaratne; R. A. Shanks, Eur Polym J 41(2005) 2980.

44. L. Jiang; M. P. Wolcott; J. Zhang, Biomacromolecules 7(2006) 199.

45. A. J. Owen; J. Heinzel; Ž. Škrbić; V. Divjaković, Polymer 33(1992) 1563.

46. S. Wang; C. Song; G. Chen; T. Guo; J. Liu; B. Zhang; S. Takeuchi, Polym Degrad Stab 87(2005) 69.

47. Yu, H; Qin, Z; Liang, B; Liu, N; Zhoub, Z; Chen, L, J. Mater. Chem. A, 1(2013) 3938

48. S. Cimmino; P. Iodice; C. Silvestre; F. E. Karasz, J Appl Polym Sci 75(2000) 746.

49. S. Vidhate; L. Innocentini-Mei; N. A. D'Souza, Polym Eng Sci 52(2012) 1367.

50. V. Sridhar; I. Lee; H. H. Chun; H. Park, Express Polymer Letters 7(2013) 320.

51. M. Kunioka; A. Tamaki; Y. Doi, Macromolecules 22(1989) 694.

52. M. Avrami, The Journal of Chemical Physics 7(1939) 1103.

53. M. Avrami, The Journal of Chemical Physics 8(1940) 212.

54. M. Avrami, The Journal of Chemical Physics 9(1941) 177.

55. F. De Santis; R. Pantani, J Therm Anal Calorim 112(2013) 1481.

56. S. Iannace; L. Nicolais, J Appl Polym Sci 64(1997) 911.

57. M. J. Fabra; A. Lopez-Rubio; J. M. Lagaron, Food Hydrocolloids 32(2013) 106.

58. J. Ambrosio-Martín; G. Gorrasi; A. Lopez-Rubio; M. J. Fabra; L. Cabedo; M.A. Lopez-Manchado; J. M. Lagaron, J Appl Polym Sci 132(2014) 42101

Figure captions

Figure 1 SEM micrographs of the cryo-fractured section obtained from PHBV films: (a) neat PHBV; (b) PHBV/BCNW 0.5 wt.%; (c) PHBV/BCNW 1 wt.% and (d) PHBV/BCNW 3 wt.%. Scale markers correspond to 10 μm.

Figure 2 TEM micrographs of PHBV-BCNW films containing 1 wt.% BCNW. Scale markers correspond to 2μm.

Figure 3 Contact transparency pictures of PHBV and PHBV/BCNW nanocomposites films.

Figure 4 ATR-FTIR spectra of the neat PHBV and nanocomposites films containing BCNW.

Figure 5 DSC first heating scan (a), cooling scan (b) and second heating scan (c) of the neat PHBV and the PHBV/BCNW nanocomposites prepared by ball-milling.

Figure 6 TGA curves of pure BCNW, pure PHBV and its nanocomposites with BCNW (a, b) and DTG curves of pure PHBV and its nanocomposites with BCNW (c, d) in air and nitrogen environments (left and right respectively). The insets are expanded views at different temperature ranges.

Figure 7 Temperature dependence of the storage modulus of the neat PHBV and the PHBV/BCNW nanocomposites prepared by ball-milling.

Figure 8 Tanδ of the net PHBV and the PHBV/BCNW nanocomposites prepared by ball-milling.

Figure 9 X-Ray diffraction patterns of neat PHBV and nanocomposites containing BCNW.

Figure 10 DSC curves of isothermal crystallization at 133 ºC, 135 ºC and 137 ºC of the PHBV/BCNW 1 wt.% nanocomposites obtained by ball-milling.

Table I. Opacity Values of Films with Different BCNC Contents

BCNW loadings (%)	Apparent Opacity
0	51.8±1.1
0.5	53.4±1.2
1	51.5±1.2
3	48.9±1.9

Table II. DSC maximum of melting (T_m), melting enthalpy (ΔH_m) and degree of crystallinity (X_c) during the first heating run, crystallization temperature (T_c) and crystallization enthalpy (ΔH_c) during the cooling run and maximum of melting (T_m) and melting enthalpy (ΔH_m) during the second heating run.

BCNW loadings (%)	**1st Heating**				**Cooling**		**2nd Heating**	
	T_{m1} (°C)	**T_{m2} (°C)**	**ΔH_m (J g^{-1})**	**X_c (%)**	**T_c (°C)**	**ΔH_c (J g^{-1})**	**T_{m1} (°C)**	**ΔH_m (J g^{-1})**
0	149.5	158.7	62.5	57.4	113.2	65.5	153.5	69.4
0.5	150.3	158.9	63.3	58.0	112.5	65.9	153.4	69.7
1	148.0	158.2	64.7	59.4	113.2	66.4	153.5	70.3
3	144.8	157.5	69.9	64.1	114.0	67.9	152.7	72.4

Table III. TGA decomposition temperature (T_d), onset temperature (T_{onset}) and the residue at 600°C for neat PHBV and its nanocomposites incorporating BCNW evaluated in air and nitrogen environment.

BCNW loadings (%)	T_d (°C)		T_{onset} (°C)		% Residue at 600 °C	
	air	N_2	air	N_2	air	N_2
0	284.2	276.0	266.7	259.6	1.4	2.4
0.5	286.1	284.8	266.9	266.3	3.4	2.6
1	282.7	283.0	264.3	265.0	3.1	2.6
3	282.9	282.2	264.3	264.1	3.2	3.5

Table IV. Effect of BCNW content on the crystallite size for (020) reflections

BCNW loadings (%)	***d*-spacing (nm)**	**Crystallite size D_{020} (nm)**	**Crystallinity Index (X_i)**
0	0.64	16.28	53.5
0.5	0.65	27.63	60.2
1	0.66	30.28	61.0
3	0.66	28.06	62.0

Table V. Avrami kinetic parameters for the crystallization of the neat PHBV and the PHBV/BCNW nanocomposites

BCNW loadings (%)	133 ºC			135 ºC			137 ºC		
	K (s^{-1})	n	$t_{1/2}$	K (s^{-1})	n	$t_{1/2}$	K (s^{-1})	n	$t_{1/2}$
0	2.5E-03	1.6	318.2	1.8E-03	1.6	442.1	1.6E-03	2.2	521.9
0.5	2.6E-03	1.6	304.4	2.0E-03	1.7	391.7	1.7E-03	1.8	470.7
1	2.4E-03	1.7	331.3	2.0E-03	1.6	392.4	1.6E-03	1.6	489.7
3	2.7E-03	1.6	298.0	2.0E-03	1. 6	395.5	1.8E-03	1.7	455.1

Table VI. Oxygen permeability values of the neat PHBV and its nanocomposites with BCNW.

BCNW loadings (%)	**OP · 10^{19} (m^3 m m^{-2} s^{-1} Pa^{-1})**
0	2.8 ± 0.1^{b}
0.5	2.2 ± 0.3^{c}
1	2.3 ± 0.2^{c}
3	2.3 ± 0.3^{c}

a-b: different superscripts within the same column indicate significant differences between samples.

Table VII. Sorption and diffusion coefficients of water vapour of PHBV and its nanocomposites with BCNW.

BCNW loadings (%)	Sorption (Ceq water (g/100g))	Diffusion (cm^2 s^{-1})
0	0.66 ± 0.03^{a}	$1.6 \pm 0.0\ e^{-8\ ab}$
0.5	0.63 ± 0.06^{a}	$1.4 \pm 0.1\ e^{-8\ b}$
1	0.68 ± 0.13^{a}	$1.0 \pm 0.1\ e^{-8\ c}$
3	0.66 ± 0.06^{a}	$1.3 \pm 0.1\ e^{-8\ b}$

a-c: different superscripts within the same column indicate significant differences between samples.

Figure 1

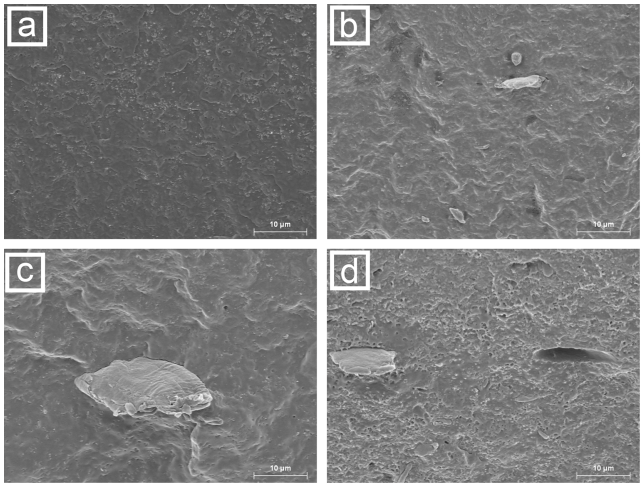

Figure 2

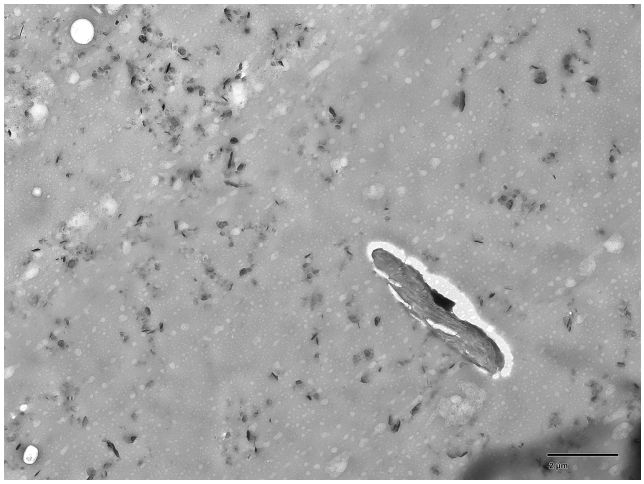

Figure 3

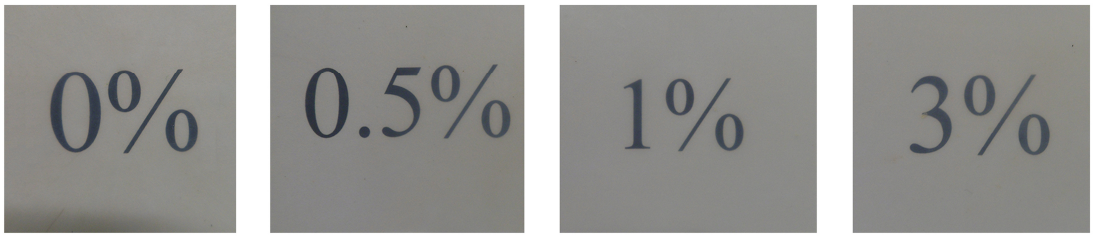

Figure 4

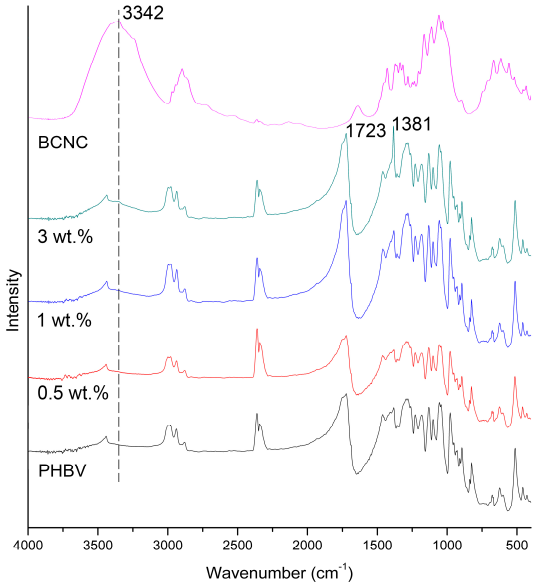
3342
1723
1381
BCNC
3 wt.%
1 wt.%
0.5 wt.%
PHBV
Intensity
4000
3500
3000
2500
2000
1500
1000
500
Wavenumber (cm-1)

Figure 5

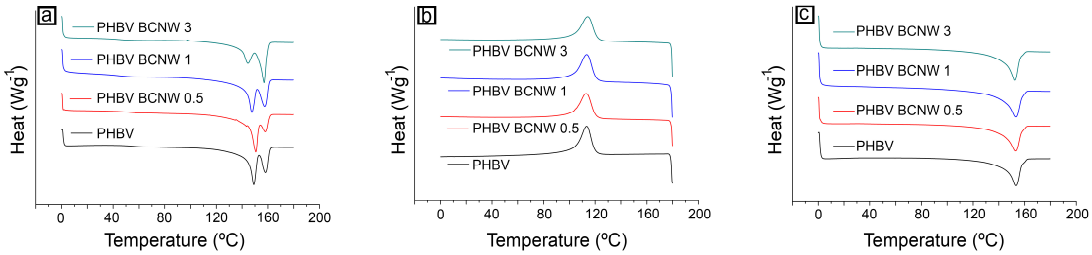
a
PHBV BCNW 3
PHBV BCNW 1
PHBV BCNW 0.5
PHBV
Heat (Wg-1)
0
40
80
120
160
200
Temperature (°C)
b
PHBV BCNW 3
PHBV BCNW 1
PHBV BCNW 0.5
PHBV
Heat (Wg-1)
0
40
80
120
160
200
Temperature (°C)
c
PHBV BCNW 3
PHBV BCNW 1
PHBV BCNW 0.5
PHBV
Heat (Wg-1)
0
40
80
120
160
200
Temperature (°C)

Figure 6

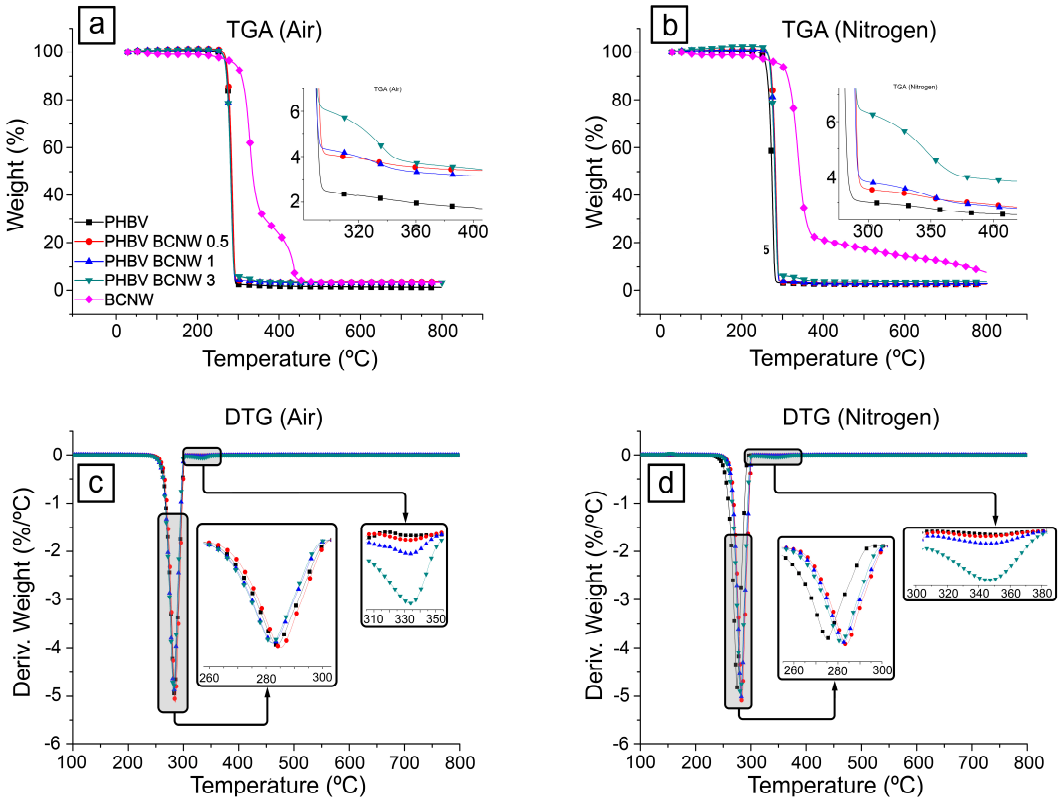
a
TGA (Air)
Weight (%)
Temperature (°C)
PHBV
PHBV BCNW 0.5
PHBV BCNW 1
PHBV BCNW 3
BCNW
b
TGA (Nitrogen)
Weight (%)
Temperature (°C)
c
DTG (Air)
Deriv. Weight (%/°C)
Temperature (°C)
d
DTG (Nitrogen)
Deriv. Weight (%/°C)
Temperature (°C)

Figure 7

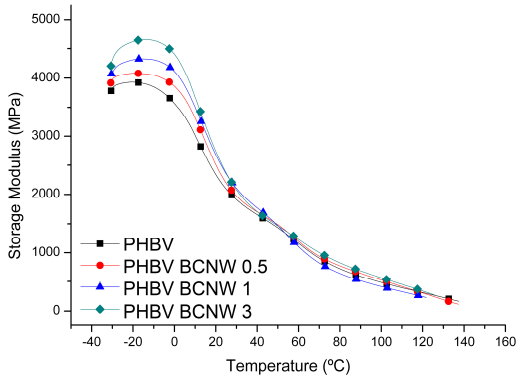
Storage Modulus (MPa)
Temperature (°C)
PHBV
PHBV BCNW 0.5
PHBV BCNW 1
PHBV BCNW 3
5000
4000
3000
2000
1000
0
-40
-20
0
20
40
60
80
100
120
140
160

Figure 8

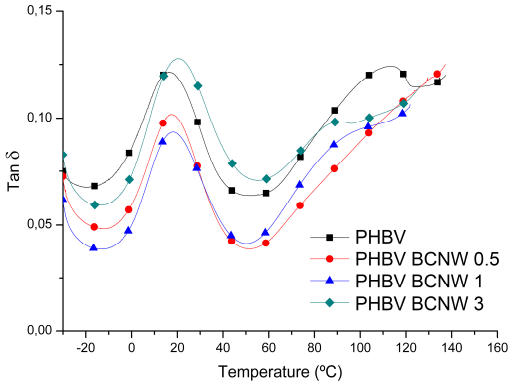
0,15
0,10
0,05
0,00
Tan δ
-20
0
20
40
60
80
100
120
140
160
Temperature (°C)
PHBV
PHBV BCNW 0.5
PHBV BCNW 1
PHBV BCNW 3

Figure 9

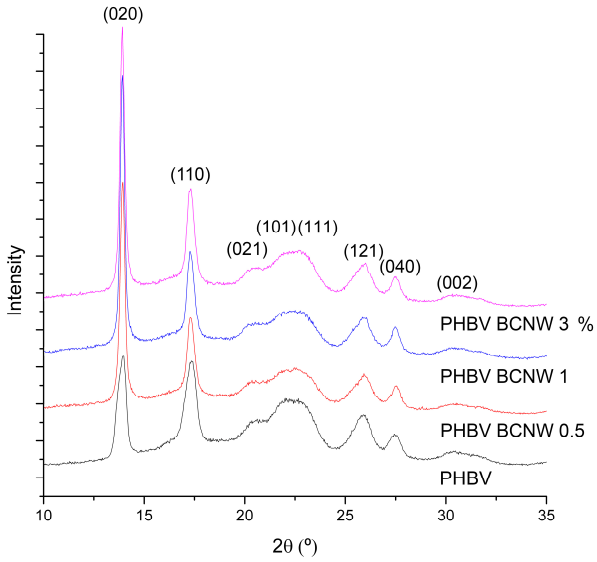
(020)
(110)
(101)(111)
(021)
(121)
(040)
(002)
PHBV BCNW 3 %
PHBV BCNW 1
PHBV BCNW 0.5
PHBV
Intensity
10
15
20
25
30
35
2θ (°)

Figure 10

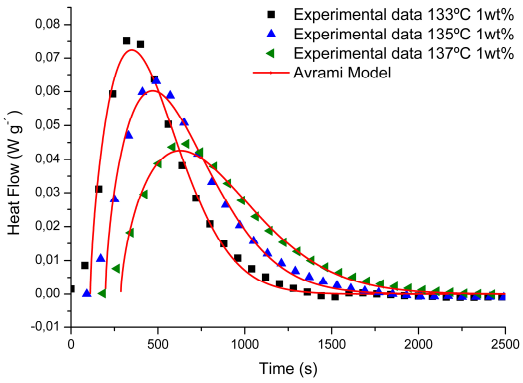
Experimental data 133ºC 1wt%
Experimental data 135ºC 1wt%
Experimental data 137ºC 1wt%
Avrami Model
Heat Flow (W g⁻¹)
Time (s)
0,08
0,07
0,06
0,05
0,04
0,03
0,02
0,01
0,00
-0,01
0
500
1000
1500
2000
2500